

CERN - PS DIVISION

CERN/PS 2002-083 (AE)

COMPUTATION OF BETATRON MISMATCH AND EMITTANCE BLOW-UP FOR MULTI-TURN EXTRACTION

R. Cappi and M. Giovannozzi

Abstract

The present version of the five-turn Continuous Transfer extraction at PS machine is based on beam slicing by means of an electrostatic septum. Recently, a novel approach has been proposed, where the beam is split into five beamlets by means of stable islands, created by sextupoles and octupoles, together with a proper tune variation. In this paper, the two approaches are compared by considering their properties in terms of equivalent optical parameters, beam emittance, and emittance after filamentation in the receiving machine (SPS) for the various slices. Analytic expressions of the relevant optical and beam parameters are derived for the present version of the Continuous Transfer, while the same quantities are estimated in the case of the novel approach via numerical simulations. Finally, the robustness of the approach based on adiabatic capture in transverse phase space is discussed with particular emphasis on tune ripple effects and variation of nonlinear elements strength.

Geneva, Switzerland

December 17, 2002

1 Introduction

In the framework of the activities to prepare the future high-intensity proton beam for the CERN Neutrino to Gran Sasso (CNGS) Project [1], a critical review of the key processes used to generate such a beam has been carried out [2], in view, possibly, of an upgrade beyond the present nominal intensity value of about 3.3×10^{13} protons per PS batch.

Among other issues, efforts have been devoted to the improvement of the present extraction scheme from PS to SPS, the so-called Continuous Transfer (CT). Such an extraction mode was developed in the mid-seventies [3] with the aim of delivering a beam to the SPS five PS turns long and with a reduced horizontal beam emittance so to overcome the SPS aperture limitation in the vertical plane¹⁾. This approach consists in slicing the beam by means of an electrostatic septum: with the tune set to 6.25 this method allows generating one continuous ribbon four-turn long plus an additional slice, represented by the beam core, for a total beam length of five PS turns. Although this extraction mode is certainly adapted to present performance, in the event of an intensity increase, a number of potential weak points appear, such as the intrinsic beam losses related with the underlying principle of this extraction mode, and also the properties of phase space matching of the different slices.

In the search for an improved extraction mode, a novel approach was proposed. In the new scenario the beam will be separated in transverse phase space by generating stable islands inside the region where the beam sits and by slowly (adiabatically) moving them towards higher amplitudes. By doing this, particles may get trapped inside islands thus generating well-separated beamlets [5, 6]. This method is potentially superior to the present one as no intercepting device is used to split the beam, hence no particle losses should occur during the extraction process. Furthermore, the extracted beam should better match the phase space structure.

In this paper two key issues are addressed: the properties of phase space matching, i.e. emittance of the extracted beam, mismatch parameters, and emittance after filamentation in the receiving machine, as well as the robustness of the novel approach against variation of the strength of the nonlinear magnetic elements used to generate the stable islands and tune ripple effects. Quantitative answers to these aspects are the necessary ingredients to evaluate and compare the performance of the different approaches. The analysis presented in this paper represents a more detailed and complete version of the results presented in Ref. [7].

The outline of the paper is the following: in section 2 the main definitions concerning the beam emittance, the computation of the betatron mismatch, optical parameters, and emittance after filamentation are presented. Also, the distributions used in the analytical computations are discussed in details. In section 3 the present CT extraction mode is analysed. Special emphasis is given on the phase space matching properties of the different slices (section 3.2) and emittance blow-up at SPS injection (section 3.3). Section 4 deals with the proposed multi-turn extraction based on island trapping: it is briefly presented (section 4.1) while the results concerning the robustness of the method and the beam characteristics at extraction are presented in details (sections 4.2 and 4.3). Finally, conclusions are drawn in section 5. Most of the analytical computations presented in this paper are collected in the Appendixes A- D

2 Betatron Mismatch in Normalised Phase Space

2.1 Definition of Mismatch Parameters

When a beam is injected into a circular machine, it may experience emittance blow-up due to a number of different phenomena. In this paper we will focus on the betatron mismatch [8, 9],

¹⁾ A special optics in the transfer line joining the PS and SPS allows exchanging the two transverse planes (in particular the emittance values) [4].

which occurs when the beam optical parameters at injection do not fit those of the circular machine. In this case, tails may grow at the expense of the beam core, thus increasing the overall beam emittance. Of course, such a behaviour is particularly harmful for high-intensity beams as they usually fill completely the machine acceptance.

To quantify the betatron mismatch, it is customary to start from the statistical definition of beam emittance ϵ and optical parameters $\bar{\alpha}, \bar{\beta}, \bar{\gamma}$ [10] in terms of the second order moments of the beam distribution [11]. By using the notation (x, x') for the physical phase space coordinates, while (\hat{x}, \hat{x}') represent normalised Courant-Snyder co-ordinates [10], the following holds:

$$\begin{aligned} \langle x^2 \rangle &= \bar{\beta} \epsilon \\ \langle x x' \rangle &= -\bar{\alpha} \epsilon \\ \langle x'^2 \rangle &= \bar{\gamma} \epsilon. \end{aligned} \quad (1)$$

In the equations quoted above the symbol $\langle \cdot \rangle$ stands for the average over the beam distribution of the specified variable. It is worthwhile mentioning that whenever the beam distribution is not centred at the origin, the second order moments in Eq. (1) are the central ones, i.e. referred to the mean value of the beam distribution. This approach is equivalent to fit an ellipse to the phase space distribution, where the fit parameters are its surface, amplitude, and orientation.

If the nominal Twiss parameters α, β, γ , i.e. those relative to the nominal optics, are used to transform Eq. (1) into normalised phase space via the well-known transformation rules [10]

$$\hat{x} = \frac{x}{\sqrt{\beta}} \quad \hat{x}' = \frac{\alpha}{\sqrt{\beta}} x + \sqrt{\beta} x', \quad (2)$$

the key relations

$$\begin{aligned} \langle \hat{x}^2 \rangle &= \frac{\bar{\beta}}{\beta} \epsilon \\ \langle \hat{x} \hat{x}' \rangle &= \left(\alpha \frac{\bar{\beta}}{\beta} - \bar{\alpha} \right) \epsilon \\ \langle \hat{x}'^2 \rangle &= \left(\alpha^2 \frac{\bar{\beta}}{\beta} - 2 \alpha \bar{\alpha} + \beta \bar{\gamma} \right) \epsilon \end{aligned} \quad (3)$$

are obtained. The value of the rms emittance can be computed by solving Eqs. (3), namely

$$\epsilon = \langle \hat{x}^2 \rangle \langle \hat{x}'^2 \rangle - \langle \hat{x} \hat{x}' \rangle^2. \quad (4)$$

The meaning of the coefficients $\bar{\beta}/\beta$ and $\alpha \bar{\beta}/\beta - \bar{\alpha}$ is clear: they measure the deviation of the 1σ contour of the beam distribution from the circular shape it should have in normalised phase space. In case of perfect matching one would have $\bar{\beta}/\beta = 1$ and $\alpha \bar{\beta}/\beta - \bar{\alpha} = 0$, implying the trivial relation $\bar{\beta} = \beta, \bar{\alpha} = \alpha$. Furthermore, it turns out that the emittance after filamentation, $\epsilon_{\text{after fil.}}$, i.e. when the circular symmetry has been restored in the receiving machine, is expressed as [9]

$$\epsilon_{\text{after fil.}} = H \epsilon, \quad \text{where} \quad H = \frac{1}{2} \left[\frac{\bar{\beta}}{\beta} + \frac{\beta}{\bar{\beta}} + \left(\alpha \sqrt{\frac{\bar{\beta}}{\beta}} - \bar{\alpha} \sqrt{\frac{\beta}{\bar{\beta}}} \right)^2 \right], \quad (5)$$

where ϵ is the initial value of the beam emittance.

2.2 Beam Distribution for the Present CT

It is customary to assume that the transverse beam distribution is a Gaussian function, namely

$$\rho_G(\hat{x}, \hat{x}') = \frac{1}{2\pi\epsilon} e^{-\frac{\hat{x}^2 + \hat{x}'^2}{2\epsilon}}, \quad (6)$$

where ϵ is the rms beam emittance. However, the presence of long, and strictly speaking infinite, tails makes some results difficult to interpret. For this reason, a second beam distribution has been considered, a so-called *quasi-parabolic* distribution (see, e.g. Ref. [12] and references therein for more details). Such a distribution does not have tails, though it is not a truncated Gaussian. It is represented by a smooth function

$$\rho_P(\hat{x}, \hat{x}', m) = \begin{cases} \frac{m+1}{2\pi\epsilon(m+2)} \left[1 - \frac{\hat{x}^2 + \hat{x}'^2}{2\epsilon(m+2)}\right]^m & \text{if } \hat{x}^2 + \hat{x}'^2 \leq 2\epsilon(m+2), \\ 0 & \text{if } \hat{x}^2 + \hat{x}'^2 > 2\epsilon(m+2). \end{cases} \quad (7)$$

where m is a parameter and ϵ the rms beam emittance. In all the computations presented in this paper $m = 5$ has been used. In Fig. 1 the comparison between a Gaussian distribution ρ_G and a quasi-parabolic one ρ_P is shown as a function of the parameter m . The difference between the

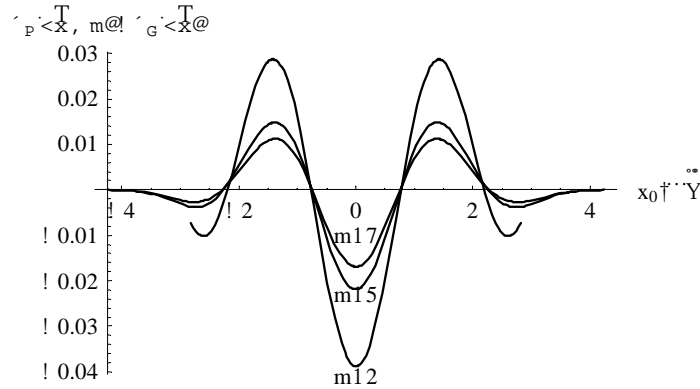


Figure 1: Comparison between Gaussian distribution function ρ_G and a quasi-parabolic one ρ_P (integration over the angular variable \hat{x}' has been performed). The difference between the two distributions is plotted as a function of $x_0/\sqrt{\epsilon}$ for different values of m .

two distributions is quite small and it decreases for increasing m , thus making it an ideal choice for the study presented in this paper.

3 Present Continuous Transfer

3.1 Basic Principle

Before describing in details the computation of the beam emittance, optical parameters, and mismatch factors for the different slices generated by the present CT, the key elements of the extraction mode, i.e. the complex system of slow and fast bumps and the slicing obtained by the action of an electrostatic septum when the horizontal tune is set to 6.25 is show in Fig. 2.

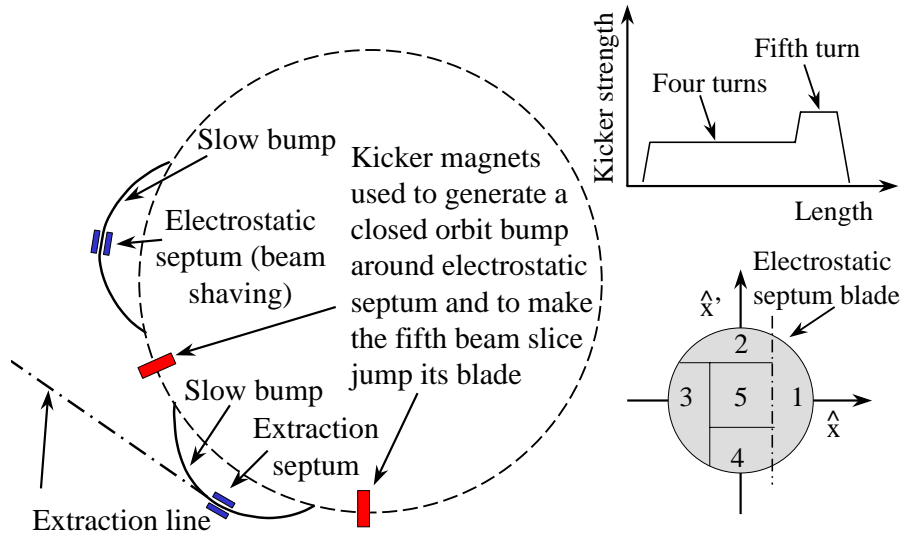


Figure 2: Principle of the CT extraction from the PS machine: the extraction scheme (left), the kicker strength as a function of time (upper left), the normalised phase space (lower right).

3.2 Analytical evaluation of emittance and beam parameters for different slices

The goal of these computations is the evaluation of the beam emittance and betatron mismatch for the different slices of the present CT. The starting point is Eq. (3). In the following, two cases will be considered with an increasing degree of complexity, namely (i) a single free parameter to be used in the generation of the five slices, and (ii) four independent parameters.

3.2.1 One free parameter

It is assumed that the position of the electrostatic septum for the first slice is the only degree of freedom of the process. This is not true in practice, but it is a useful assumption for visualising the results. This implies that a number of artificial symmetries are generated, e.g. the second and third slices have the same shape, hence the same emittance; the fourth slice is symmetric with respect to the \hat{x}' axis, thus satisfying $\alpha\bar{\beta}_4/\beta - \bar{\alpha}_4 = 0$; the fifth slice is a square, which implies that it is perfectly matched.

The computation of the relevant quantities under study can be carried out in closed analytical form also taking into account the dependence on the electrostatic septum position. The results are reported in Appendix B for the case of a Gaussian beam distribution (the special functions used in the analytical computations are listed in Appendix A). It is worthwhile stressing that the special form of the beam distribution (6), i.e. $\rho_G(\hat{x}, \hat{x}') = \rho_G(\hat{x}) \rho_G(\hat{x}')$, together with the shape of the integration domain used in the computation of $\bar{\beta}_i/\beta$, and $\alpha\bar{\beta}_i/\beta - \bar{\alpha}_i$, has the consequence of producing $\langle \hat{x} \hat{x}' \rangle = 0$ for all the beam slices. This artificial effect is not generated by the quasi-parabolic distribution.

The results of the analytical computations are shown in Fig. 3 where the emittance and the mismatch factors for the different slices are shown for both types of beam distributions as a function of the position of the electrostatic septum at the first slice. The two beam distributions do generate rather similar results. The main discrepancy is visible in the plot of the beam emittance for the various slices where the effect of the long tails is clearly visible. To verify that the Gaussian tails do not introduce non-physical results, e.g. non zero limiting value for the beam emittance, the asymptotic limit of the analytical expressions presented in Appendix B has been computed. The results are reported in Appendix D, based on the definitions presented in Appendix C. The asymptotic limits prove that the computed beam emittance converges to zero,

as it should. However, the Gaussian tails make such a convergence so slow that a rather large beam emittance is corresponding to a phase space region where, in reality, almost no beam is present.

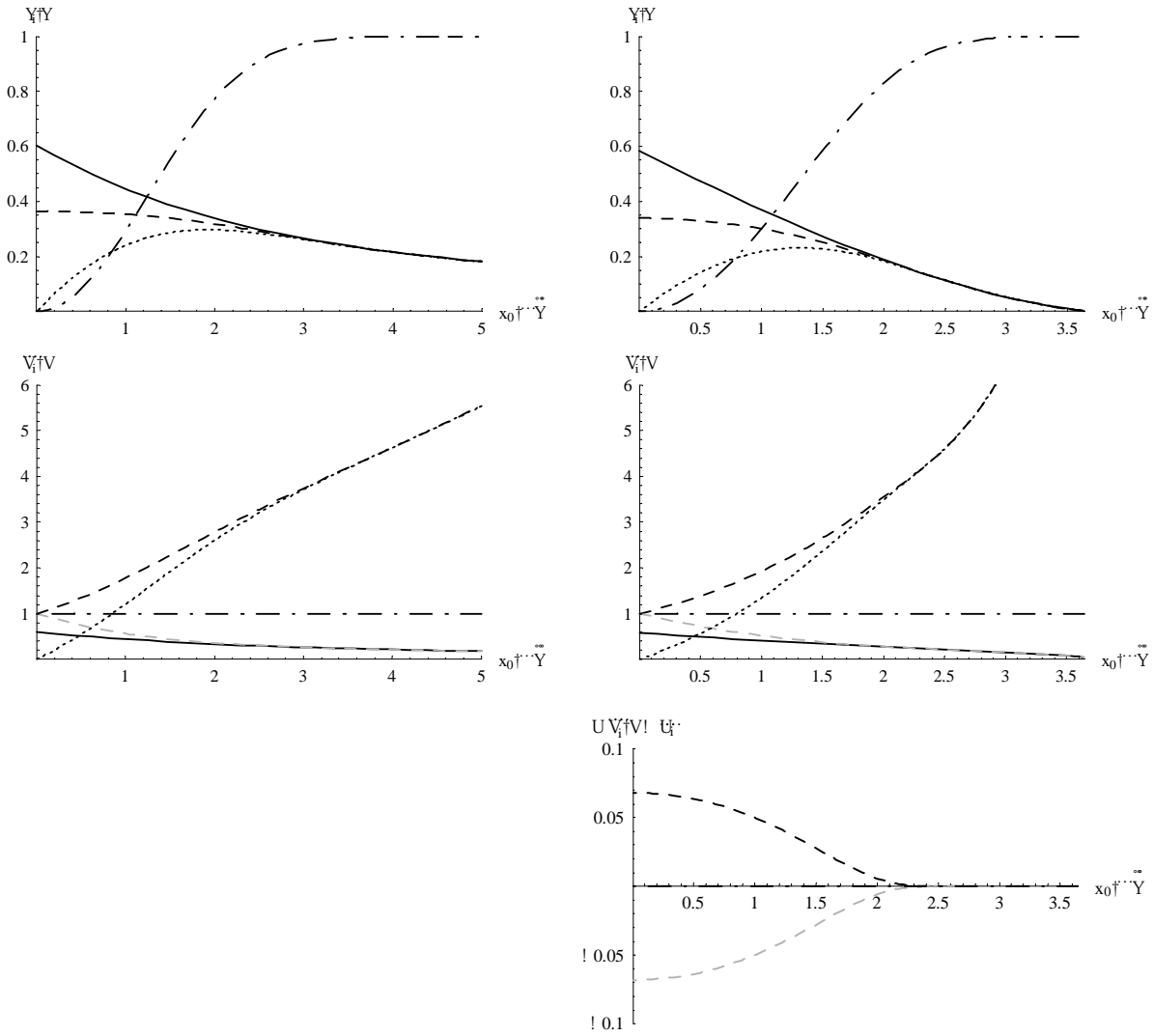


Figure 3: Relative emittance ϵ_i/ϵ (upper), $\bar{\beta}_i/\beta$ (centre), and $\alpha \bar{\beta}_i/\beta - \bar{\alpha}_i$ (lower) for the five slices as a function of $x_0/\sqrt{\epsilon}$ (first slice solid, second dashed, third light dashed, fourth dotted, fifth dot-dashed). The two columns refer to a Gaussian distribution (left) and a quasi-parabolic one (right). The plot of $\alpha \bar{\beta}_i/\beta - \bar{\alpha}_i$ for a Gaussian beam distribution is not shown as it is always equal to zero. The second and third slice have the same value of ϵ_i/ϵ .

Apart from this fact, the most striking feature is the difference in beam emittance for the various slices: from the plot it is clear that by using only one free parameter it is not possible to make the slices having the same beam emittance. Furthermore, also the other mismatch factors confirm that the different slices behave differently and that the betatron mismatch can be quite large.

3.2.2 Four free parameters

In reality, the performance of the kickers used for the CT extraction allows controlling the shape of each single slice, hence, in the second case, four free parameters, representing the

position of the electrostatic septum for the first four turns, have been considered. With the increased number of degrees of freedom it is possible to closely simulate what is done in reality, namely set the position of the electrostatic septum so to have the same extracted intensity for each slice. The analytic expressions become too involved to be of any practical use. Hence, the approach consisted in determining the electrostatic septum position for the i th slice so to have an intensity equal to $1/5$ of the initial one, provided the previous positions were already determined by a similar condition on the corresponding slices.

In addition a refined approach has been studied, consisting in determining the septum positions so as to equalise the emittances of the five slices. Of course, this second attempt is not possible in practice as no device is available to measure the beam emittance of each extracted turn. In this case, a mixed, analytical and numerical approach has been used as no *a priori* estimate of the common value of the beam emittance is known. Hence, the analytical formulae have been used to compute the septum positions so to obtain $\epsilon_i/\epsilon = \varepsilon \quad i \leq 4$, where ε is an arbitrary value. Then, the resulting emittance of the fifth slice, ϵ_5/ϵ , has been computed, thus obtaining a curve $\epsilon_5/\epsilon = f(\varepsilon)$ in dependence of the chosen value of ε . The common value of the emittance can be found by solving numerically the equation $f(\varepsilon) = \varepsilon$. In Fig. 4 (left) the resulting curves $\epsilon_5/\epsilon = f(\varepsilon)$ for the Gaussian and quasi-parabolic distributions are shown. In the right part, the sum of the emittances of the five slices is plotted as a function of ε . The common

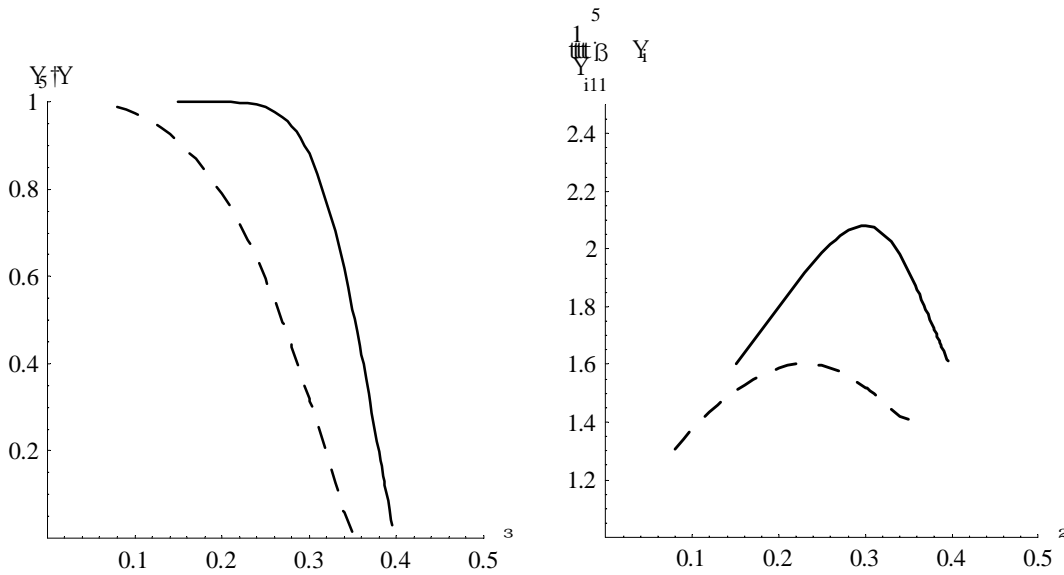


Figure 4: Relative emittance of the fifth slice ϵ_5/ϵ (left) and sum of the relative emittances of the five slices (right) as a function of ε , the common value of the relative emittance of the first four slices (solid line Gaussian, dashed quasi-parabolic distribution).

value of the extracted beam emittance is $\epsilon_i/\epsilon \approx 0.365$ for a Gaussian beam distribution, while for a quasi-parabolic one it is $\epsilon_i/\epsilon \approx 0.303$. This shows that the rough estimate of the emittance of the extracted slices obtained by simply dividing by the number of slices. i.e. $1/5$, does not fit with the outcome of the computations presented here. The discrepancy originates from the definition of beam emittance, where not only the surface in phase space but also the beam distribution, via the second-order moments, has to be taken into account. Indeed, the shape of the curve $\epsilon_5/\epsilon = f(\varepsilon)$ is qualitatively the same for both beam distributions. Interestingly enough, the total beam emittance of the five slices is considerably larger than the initial beam emittance, the effect being more pronounced for the Gaussian distribution.

Finally, some more insight can be gained by looking at the way the beam is sliced according to whether intensities or emittances are equalised. In Fig. 5 the shapes of the five slices are shown for both beam distributions. In the case of a Gaussian distribution, the dashed circle

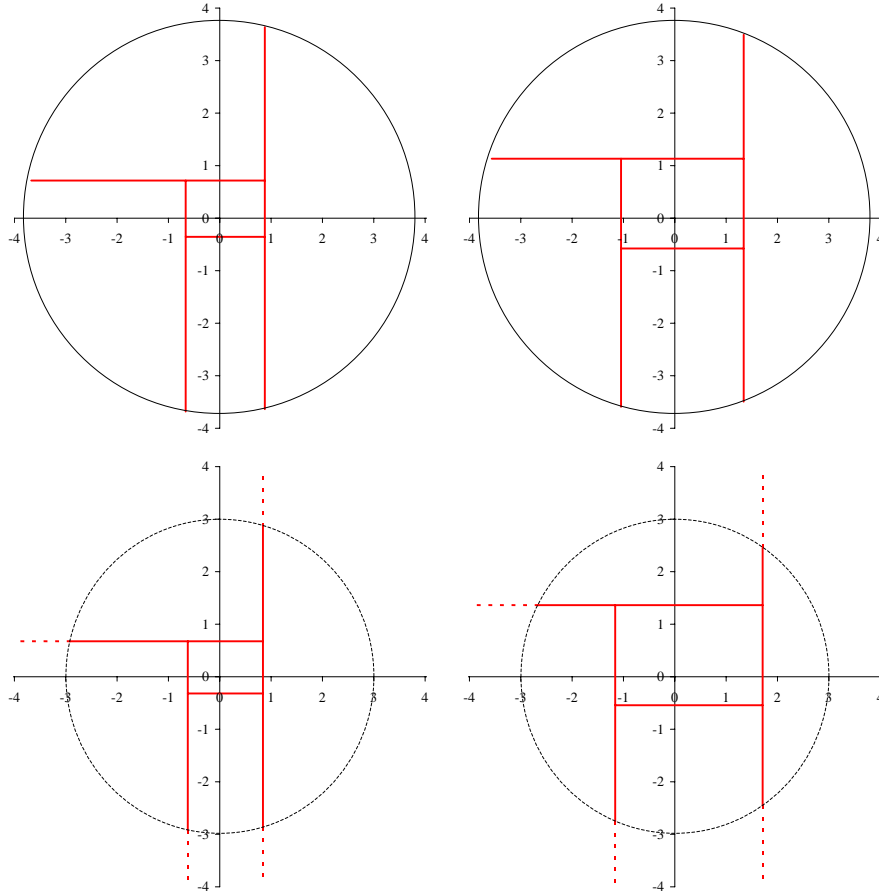


Figure 5: Shape of the five slices for the present CT in normalised phase space (\hat{x}, \hat{x}') according to whether intensities (left) or emittances (right) have been equalised. The results for a quasi-parabolic distribution are shown in the upper part, while those for a Gaussian distribution are plotted in the lower part. The solid circle represents the locus where the quasi-parabolic distribution reaches zero (at $\sqrt{14}\sigma$), while the solid circle represents the 3σ contour in the Gaussian case.

represents the 3σ contour, while for the quasi-parabolic one, the solid circle represents the line where the distribution reaches the zero value. At least qualitatively, the two distributions reveal similar features. The size of the central part shrinks when the intensities have to be the same: this is a direct consequence of the fact that most of the beam is near the centre in phase space, and hence, a small region contains a large fraction of particles. However, when the emittances have to be the same, a larger region has to be considered for the fifth slice, as the beam emittance is defined in terms of second order moments and the core of the beam has a rather small emittance. One observes that for both distributions the two approaches are not compatible: minimising the extracted beam emittances do not equalise intensities and vice-versa. To illustrate this point, the numerical results are summarised in Table 1. A clear feature is apparent: by equalising one quantity (intensity or emittance) the other shows huge variations between the different slices. The most stable case seems to be the one where equal intensity is imposed: the extracted beam emittance differs by only a factor of three between the first and the last slice. Of course, by

		Beam parameters	Slice				
			#1	#2	#3	#4	#5
Equal I	Gaussian	ϵ_i/ϵ	0.4676	0.3753	0.3651	0.2231	0.1148
		$\bar{\beta}_i/\beta$	0.4676	1.5533	0.6828	0.7445	1.4464
		$\alpha \bar{\beta}_i/\beta - \bar{\alpha}_i$	0	0	0	0	0
	Quasi-par.	ϵ_i/ϵ	0.3940	0.3347	0.3272	0.2269	0.1316
		$\bar{\beta}_i/\beta$	0.4321	1.6745	0.6391	0.8171	1.4191
		$\alpha \bar{\beta}_i/\beta - \bar{\alpha}_i$	0	0.0532	1.5700	0.0049	-0.0003
Equal ϵ	Gaussian	I_i/I (10^{-2})	4.6759	8.2613	11.2177	24.4648	51.6946
		$\bar{\beta}_i/\beta$	0.3650	2.2610	0.4965	1.3957	1.3957
		$\alpha \bar{\beta}_i/\beta - \bar{\alpha}_i$	0	0	0	0	0
	Quasi-par.	I_i/I (10^{-2})	9.4750	12.5759	13.7345	22.2097	42.0048
		$\bar{\beta}_i/\beta$	0.3698	2.2055	0.4936	1.3212	1.3496
		$\alpha \bar{\beta}_i/\beta - \bar{\alpha}_i$	0	0.0359	2.0298	0.0097	-0.0012

Table 1: Summary of the beam parameters ϵ_i/ϵ , $\bar{\beta}_i/\beta$, $\alpha \bar{\beta}_i/\beta - \bar{\alpha}_i$ and intensity I_i for the five slices of the present CT extraction. For the case of equal emittances, the common value for a Gaussian distribution is $\epsilon_i/\epsilon \approx 0.365$, while for a quasi-parabolic distribution $\epsilon_i/\epsilon \approx 0.303$.

slightly reducing the intensity of the first slice and increasing that on the last two slices more balance may be found. Also, less extreme results are observed using a quasi-parabolic distribution. Finally, it is worthwhile pointing out that the emittance ratio of the order of 0.3, as is the case for a quasi-parabolic distribution and for equal intensities, is in rather good agreement with experimental measurements [13].

3.3 Injection mismatch into the SPS

The considerations presented in the previous sections refer to the beam at extraction from the PS machine. Obviously, the most relevant quantity in the performance evaluation is the emittance after filamentation, i.e. after injection into the SPS. Different physical effects may contribute to emittance dilution, such as steering errors, dispersion mismatch and betatron mismatch [8, 9]. From the previous analysis, it turns out that the five slices have different position and angle at PS extraction. However, a correction dipole is installed in the TT2 transfer line to compensate, at least partially, for these small differences. Therefore, this source of emittance blow-up will be neglected in the following as well as the dispersion mismatch and only the betatron mismatch will be taken into account.

Figure 6 shows the factor H_i as a function of the electrostatic septum position for the simple case of a single free parameter for both beam distributions. As already stressed in the previous sections, the results are qualitatively the same for both distributions. Rather large values

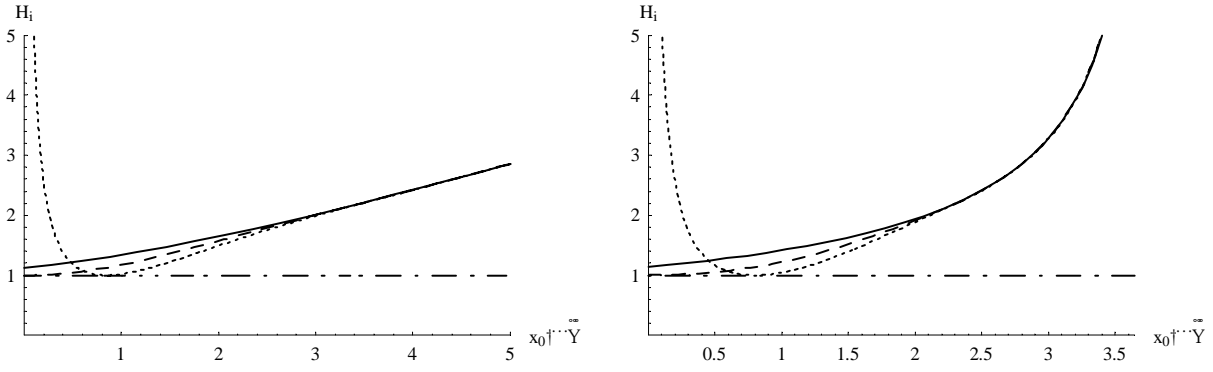


Figure 6: Emittance blow-up factor H_i for four of the five slices as a function of $x_0/\sqrt{\epsilon}$ (first slice solid, second dashed, fourth dotted, fifth dot-dashed). The two plots refer to a Gaussian distribution (left) and a quasi-parabolic one (right). Due to the symmetries introduced by the single free-parameter, $H_2 \equiv H_3$.

(up to a factor of two) for H_i are obtained. The same type of analysis described in the previous section, allows obtaining the mismatch factors H_i in the case of four independent parameters and for two different approaches, namely same intensities or same extracted beam emittances for the five slices. The numerical values of H_i are reported in Table 2. There, also the value of $\epsilon_{\text{after fil.}}/\epsilon$ is listed for each slice. Both approaches generate quite large blow-up factors (up to

		Beam parameters	Slice				
			#1	#2	#3	#4	#5
Equal I	Gaussian	H	1.3031	1.0985	1.0737	1.0439	1.0689
		$\epsilon_{\text{after fil.}}/\epsilon$	0.6093	0.4123	0.3920	0.2329	0.1227
	Quasi-parabolic	H	1.3732	1.1367	1.1046	1.0205	1.0619
		$\epsilon_{\text{after fil.}}/\epsilon$	0.5410	0.3805	0.3614	0.2316	0.2397
Equal ϵ	Gaussian	H	1.5522	1.3517	1.2553	1.0561	1.0561
		$\epsilon_{\text{after fil.}}/\epsilon$	0.5666	0.4934	0.4582	0.3855	0.3855
	Quasi-parabolic	H	1.5557	1.3297	1.2617	1.0391	1.0453
		$\epsilon_{\text{after fil.}}/\epsilon$	0.4714	0.4029	0.3823	0.3148	0.3167

Table 2: Summary of the mismatch factor H_i and emittance after filamentation for the different slices of the present CT extraction.

30 – 50 %). However, the overall ratio between $\epsilon_{\text{after fil.}}$ and beam emittance before extraction is at maximum of the order of 0.5 – 0.6 depending on the distribution and the approach used. The Gaussian distribution seems to generate larger values of H_i and $\epsilon_{\text{after fil.}}$ than the quasi-parabolic one. Equalising the intensity of the five extracted slices generates a better situation than having equal emittances.

4 The Novel Extraction Mode

4.1 Basic principle

An alternative extraction method has been proposed [5, 6] aiming at improving the weak points of the present CT extraction, namely beam losses on the electrostatic septum and betatron matching of the extracted particles. The details of the novel extraction mode, based on adiabatic capture of charged particles in stable islands of transverse phase space can be found in Refs. [5, 6]. The results presented in the following sections are obtained by inducing a linear tune variation so to sweep through the fourth-order resonance. The model used in the numerical simulations is a Hénon-like map

$$\begin{pmatrix} \hat{X}_{n+1} \\ \hat{X}'_{n+1} \end{pmatrix} = R(2\pi\nu_n) \begin{pmatrix} \hat{X}_n \\ \hat{X}'_n + \hat{X}_n^2 + \kappa \hat{X}_n^3 \end{pmatrix}, \quad (8)$$

where (\hat{X}, \hat{X}') are obtained from the Courant-Snyder [10] co-ordinates (\hat{x}, \hat{x}') by means of the non-symplectic transformations

$$\hat{X} = \frac{1}{2} K_2 \beta_H^{3/2} \hat{x} \quad \hat{X}' = \frac{1}{2} K_2 \beta_H^{3/2} \hat{x}', \quad \text{with} \quad K_l = \frac{L}{B_0 \rho} \frac{\partial^l B_y}{\partial x^l}, \quad (9)$$

K_2 (K_3) being the integrated sextupole (octupole) gradient, L the length of the nonlinear element, B_y the vertical component of the magnetic field, $B_0 \rho$ the magnetic rigidity of the charged particle, and β_H the value of the horizontal beta-function at the nonlinear elements location. $R(2\pi\nu_n)$ is a 2×2 rotation matrix of angle ν_n (the fractional part of the horizontal tune), and κ is expressed as

$$\kappa = \frac{2}{3} \frac{K_3}{\beta_H K_2^2}. \quad (10)$$

The final result is shown in Fig. 7 where the beam distribution during the capture process is reported, and in Fig. 8 where the projection of the final beam distribution is shown. The value of κ used to generate the data shown in Figs. 7, 8 is -1.6 .

Considering typical PS parameters, such as $\beta_H \approx 20.4$ m and $\epsilon_H(2\sigma) \approx 22 \mu\text{m}^2$, together with the parameters used in the numerical simulations, i.e. $\sigma = 0.037$ and $\kappa = -1.6$, then $K_2 \approx 0.88 \text{ m}^{-2}$ and $K_3 \approx 122.57 \text{ m}^{-3}$ are the values necessary for trapping and splitting the beam at 14 GeV/c. Both K_2 and K_3 are well within limits of available PS hardware. Also, the conversion factor between \hat{X} and standard physical co-ordinate x is easily found from Eq. 9. The numerical value of the conversion factor is about 0.11 m. Hence, the separation between the centre of the core and that of the right-most island is about 3.3 cm (see Ref. [15] for more details).

The proposed method should allow extracting the beam with better betatron matching. Furthermore, the first four beamlets have exactly the same beam parameters as the stable island used to extract the beam determines them. However, for the sake of completeness and to illustrate the behaviour of the proposed method, relevant quantities such as beam emittance, mismatch factors, and H -factor will be shown for all five structures (see the four stable islands plus the region around the origin in Fig. 7, lower right). To this aim the islands will be labelled starting from the central upper one and rotating clockwise, with island number five the central part.

²⁾ This value of the horizontal emittance is the reference value for high-intensity beams, issued from acceptance measurements performed in the past [2].

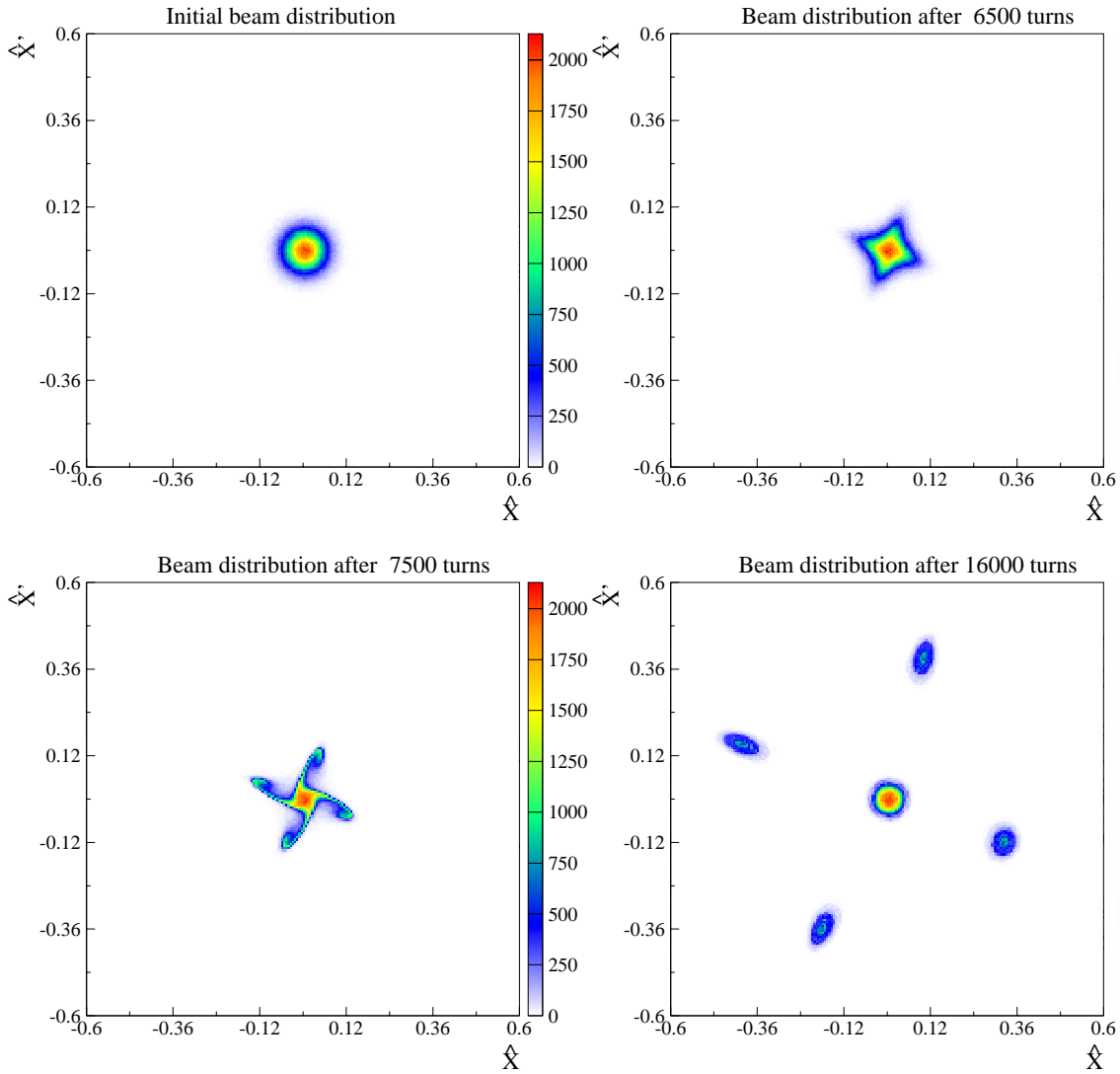


Figure 7: Evolution of the beam distribution during the trapping process with four islands. Each plot represents 4.9×10^5 points. The initial Gaussian distribution is centred on zero and has $\sigma = 0.037$. The value of κ is -1.6 .

4.2 Robustness of the proposed method

4.2.1 Variation of nonlinear elements strength

A key issue is the robustness of the novel method against variation of the strength of nonlinear elements. In fact, small deviations of K_2 , K_3 from their nominal values might change the islands parameters, thus modifying the extracted beam emittance and the capture efficiency. Numerical simulations allowed testing this point. By using the nominal model, the value of the parameter κ , defined in terms of sextupolar and octupolar strength, has been changed, without varying any other parameter (functional dependence of the tune variation on the turn number and initial beam emittance). The results are shown in Fig. 9. The data concerning all four islands are shown to illustrate the differences between the various phase space structures. However, it should be emphasised that for the actual beam extraction, only one island will be used which will make the first four beamlets exactly equivalent as far as the optical and beam parameters are concerned. Both $\bar{\beta}_i/\beta$ and $\alpha \bar{\beta}_i/\beta - \bar{\alpha}_i$ do not deviate considerably from the perfectly matched values: only the fourth island seems to differ from the others. Also the dependence on κ is mild and smooth. As far as the relative emittance is concerned, the four islands have the same behaviour, showing a sensible dependence on the value of κ . However, this fact is not

at all surprising, as κ dictates the island size [14]. It is important to stress the fact that even for this novel approach, the extracted beam emittance is about 0.4 – 0.45 times smaller than that of the circulating beam (for the last beamlet, a more favourable value is obtained for the first four beamlets), comparable with the value for the present CT extraction obtained by the computations presented in the previous sections.

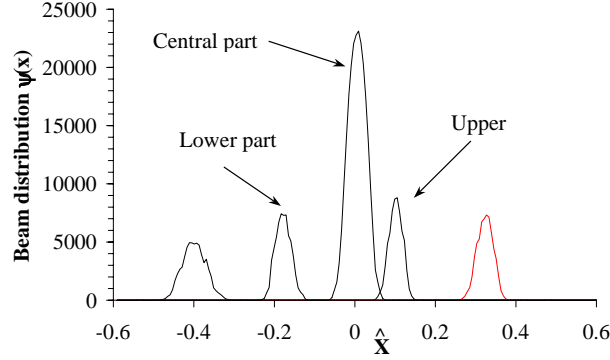


Figure 8: Beam distribution function at the end of the capture and transport process, for all five beam slices shown in Fig 7 at the end of the capture process.

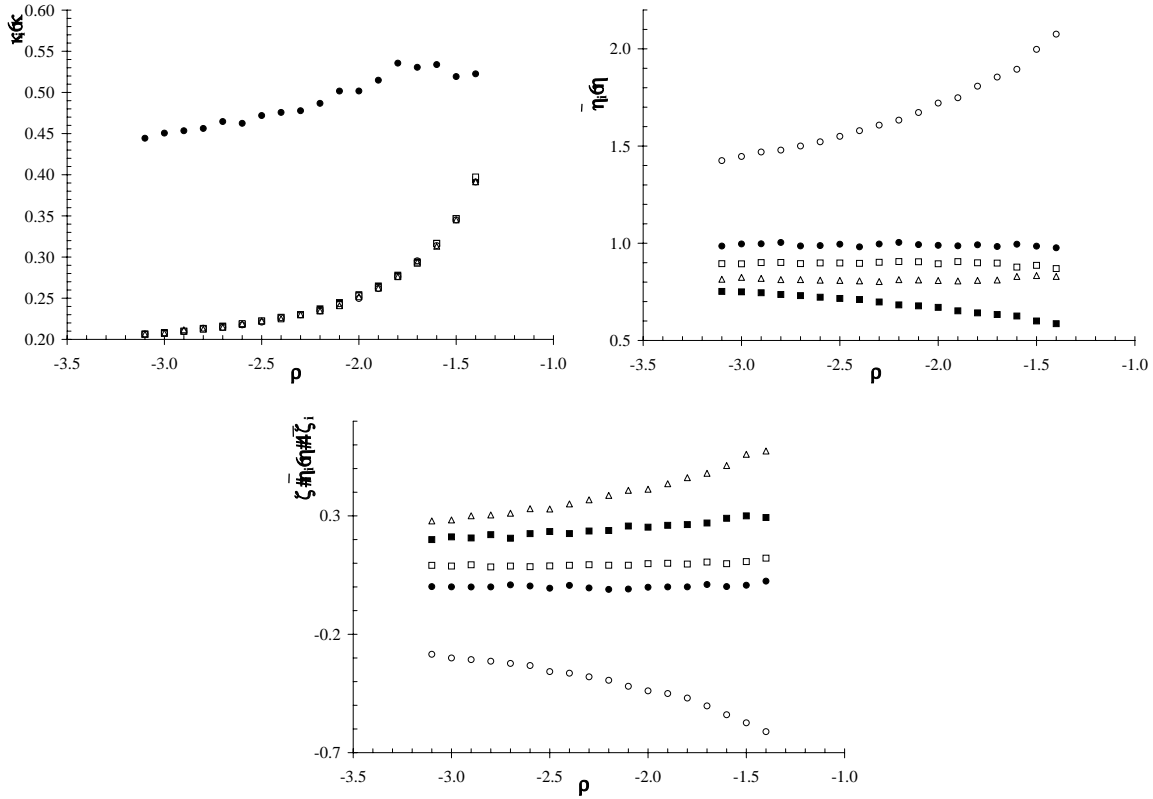


Figure 9: Properties of the five beamlets vs κ for the novel extraction mode based on adiabatic capture: relative beam emittance ϵ_i/ϵ (upper left), mismatch factor $\bar{\beta}_i/\beta$ (upper right), and mismatch factor $\alpha \bar{\beta}_i/\beta - \bar{\alpha}_i$ (lower centre) (black square first, open square second, open triangle third, open circle fourth, black circle fifth beamlet).

4.2.2 Tune ripple

Contrary to the present CT, the proposed technique might suffer from tune ripple during the delicate phase of adiabatic capture. In fact, a periodic modulation of the nominal tune may

generate particles' diffusion resulting in emittance blow-up (see Refs. [16, 17, 18] as an example of some accelerators physics issues related with modulational diffusion and Ref. [19] for a general review of the problem). The effect of tune ripple consists in periodically displacing the islands and, at a smaller level, also varying their size. Numerical simulations were performed to test this issue. The model (8) has been modified by adding a periodic tune modulation to the necessary linear tune variation.

$$\nu_n = \bar{\nu}_n [1 + \Delta\nu \cos(2\pi n f_{\text{ripple}} + \phi)], \quad (11)$$

where $\bar{\nu}_n$ represents the nominal time-dependence of the tune, $\Delta\nu$, f_{ripple} , ϕ are amplitude, frequency (properly converted from Hertz into turns), and phase of the ripple, respectively. Different values of the frequency f_{ripple} and of $\Delta\nu$ have been used in the simulations. In Fig. 10 the final result of the adiabatic capture is shown, together with the tune curve.

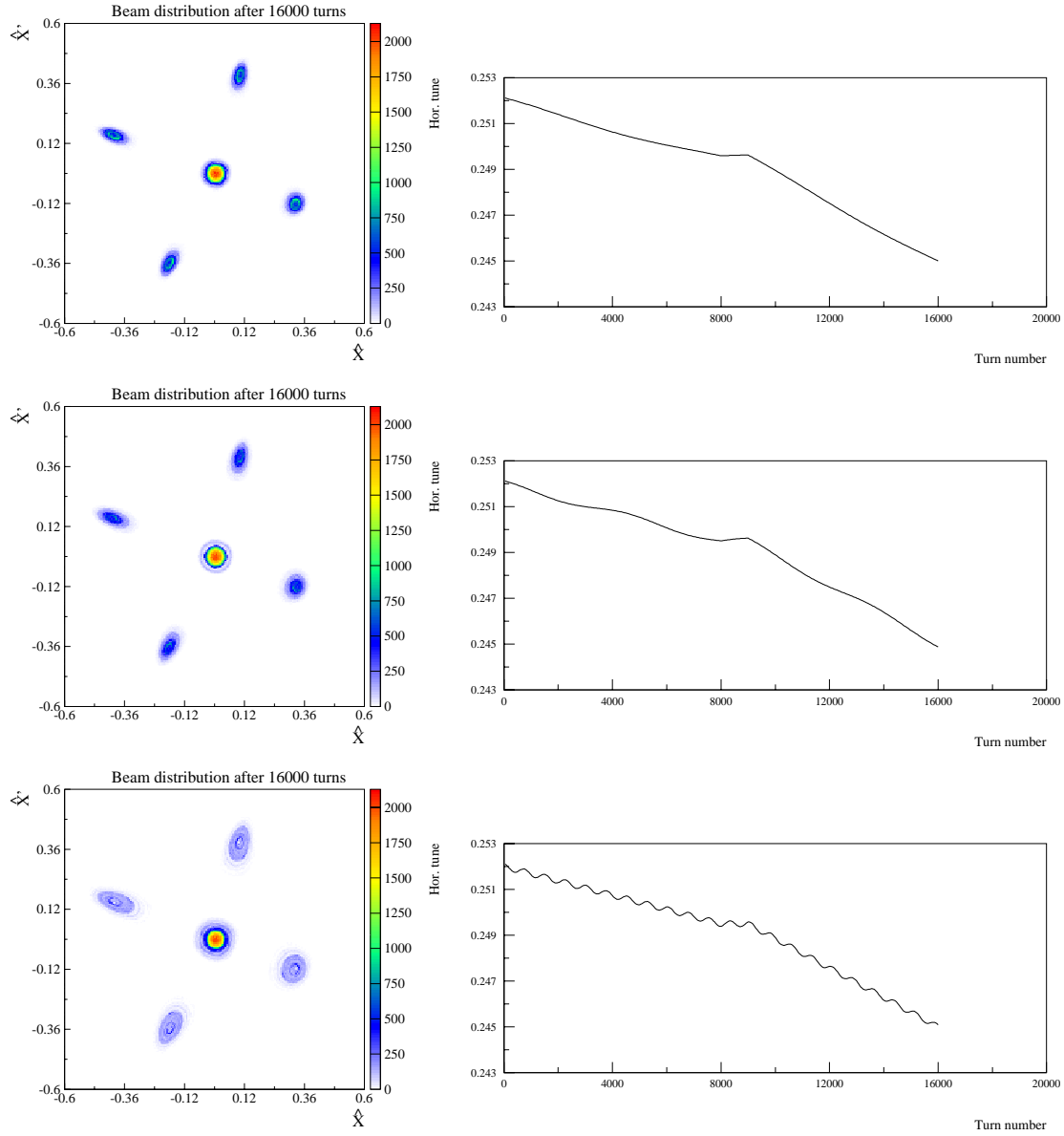


Figure 10: The generated beamlets at the end of the capture process (left) for three different ripple frequencies, 50 Hz (upper), 100 Hz (centre), and 600 Hz (lower). The tune variation is shown on the right. The tune ripple amplitude $\Delta\nu$ is 5×10^{-4} in all the cases.

It is clearly seen that the higher-frequency ripple has a bigger effect on the five beamlets: in these cases their shape is almost unchanged, but the size is increased. Furthermore, the density is proportionally decreased as it is evidenced by the lighter colour. Detailed numerical simulations confirmed that the optical parameters do not depend strongly on the presence of ripple and the value its characteristics parameters. Furthermore, the four beamlets corresponding to the four stable islands experience a rather similar emittance blow-up, higher than the one of the beam core. As an example, ϵ_1/ϵ and ϵ_5/ϵ as a function of the ripple amplitude are shown in Fig. 11. Different ripple frequencies have been tested. The case corresponding to absence of

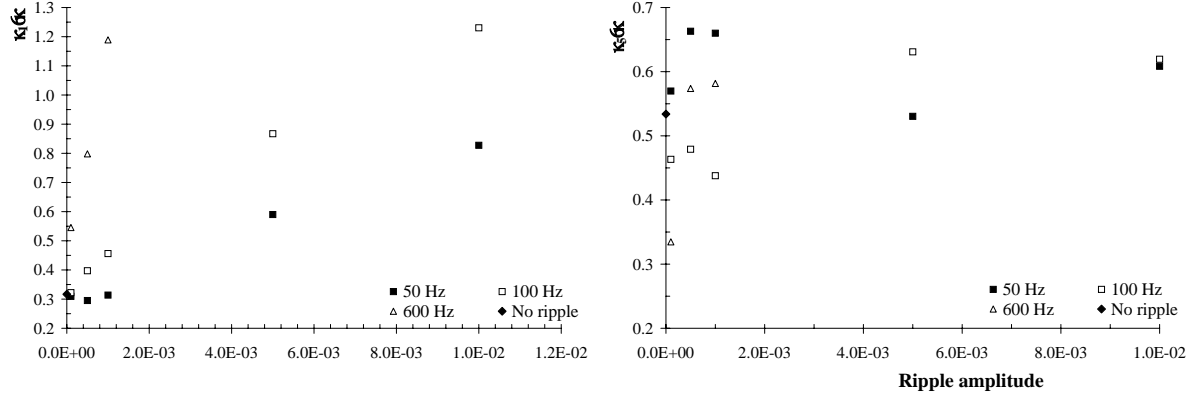


Figure 11: relative emittance ϵ_i/ϵ for the first beamlet (left) and for the core (right), as a function of the ripple amplitude for different ripple frequencies.

tune ripple is also shown as a reference. It is quite natural to observe that the lower frequencies have a smaller impact on the beam characteristics, as they act for a shorter time during the adiabatic capture process. Also, for 50 and 100 Hz, the amplitude dependence is quite smooth and regular. On the other hand for 600 Hz, the relative emittance shows a sudden increase already for quite small ripple amplitudes, while it reaches a sort of saturation immediately after.

4.3 Injection mismatch into the SPS

As it was done for the present version of the CT extraction, the blow-up after injection in the SPS was computed also for the proposed extraction. In Fig. 12 the factor H_i for the different beamlets is shown as a function of the parameter κ . Again, the dependence on the strength of

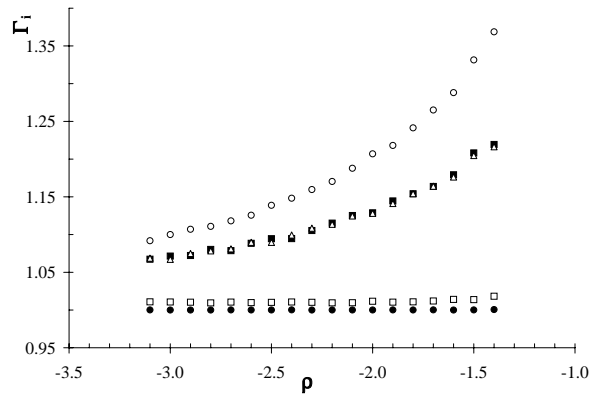


Figure 12: Emittance blow-up factor H for the five beamlets as a function of κ (black square first, open square second, open triangle third, open circle fourth, black circle fifth beamlet).

the nonlinear elements is quite smooth. Furthermore, the absolute value of H_i is much smaller than in the case of the present CT extraction (see Fig. 6). In this respect, the proposed approach seems to be superior to the CT. When tune ripple is taken into account, the fact that it does not affect very much the optical beam parameters means that the mismatch at injection will be small too.

5 Conclusions

In this paper the present CT extraction has been discussed in detail. The process of beam slicing has been reviewed and analytical results concerning the optical parameters of the various beam slices have been derived. Different models for the beam distribution have been used and the dependence of the results on the form of the chosen distribution discussed thoroughly. Furthermore, the emittance blow-up after injection in the receiving machine has been discussed under the assumption that only betatron mismatch is the relevant perturbing effect.

Similarly, computations based on extensive numerical simulations have been performed for a novel extraction method, recently proposed as a possible replacement for the CT. Such a method is based on adiabatic capture of charged particles inside stable islands of transverse phase space. Not only the optical and beam properties of the generated beamlets have been computed, but also the robustness of the proposed method against variation of the key parameters, i.e. the strength of the nonlinear elements and the presence of tune ripple, has been tested.

The proposed method seems to be superior to the present CT as far as optical parameters matching and emittance blow-up after filamentation are concerned. The optical characteristics of the extracted beamlets do not depend strongly on the strength of the nonlinear elements, sextupoles and octupoles, used to create the islands. Of course, the emittance does depend strongly on the sextupoles and octupoles parameters, but this is an intrinsic property of the method. As far as the tune ripple is concerned, numerical simulations indicate that it influences mainly the resulting beam emittance, the optical parameters of the beamlets being almost unaffected. Additional numerical simulations, performed on a realistic model of the PS machine including also the details of the measured ripple frequencies and amplitudes affecting the main quadrupoles, should clarify the effect, allowing also a more quantitative analysis.

It is worthwhile pointing out that a number of issues are still to be investigated for the novel extraction method, such as the different intensity of the five beamlets and the emittance ratio of the extracted beamlets with respect to the beam before extraction. In addition, some effects have been neglected in the simulations presented here, e.g. synchrotron motion, coupling between transverse and longitudinal dynamics, and high-intensity effects: a detailed analysis of their influence on the adiabatic capture has to be quantified carefully.

Finally, we would like to mention that the central process of the novel extraction technique, namely adiabatic capture into stable islands in transverse phase space, has been confirmed by a series of experimental results obtained at the PS machine, where a single-bunch of low-intensity was successfully split into five beamlets [20].

Acknowledgements

We would like to thank for many useful and stimulating discussions E. Métral (who also draw our attention to the form of the quasi-parabolic distribution function in Ref. [12]), M. Martini, and R. Steerenberg. We would also like to express our gratitude to K. Schindl for a careful reading of the manuscript and corrections.

References

- [1] K. Elsener (Ed.) et al., “The CERN Neutrino Beam to Gran Sasso (Conceptual Technical Design)”, *CERN* **98-02** (1998).
- [2] R. Cappi (Ed.), K. Cornelis, J.-P. Delahaye, R. Garoby, H. Haseroth, K. Hübner, T. Linnecar, S. Myers, K. Schindl, C. Wyss, “Increasing proton intensity of PS and SPS”, *CERN-PS (AE)* **2001-041** (2001).
- [3] C. Bovet, D. Fiander, L. Henny, A. Krusche, G. Plass, in *1973 Particle Accelerator Conference*, edited by D. W. Dupen (IEEE, New York, 1973) p. 438.
- [4] L. R. Evans, “A Phase Plane Exchange Section for the SPS Antiproton Injection Beam Line”, *CERN SPS (DI)* **80-2** (1980).
- [5] R. Cappi, M. Giovannozzi, *Phys. Rev. Lett.* **88**, (2002) 104801.
- [6] R. Cappi, M. Giovannozzi, “Adiabatic Capture of Charged Particles in Islands of Phase Space: a new Method for Multi-Turn Extraction”, *CERN-PS (AE)* **2002-014** (2002).
- [7] R. Cappi, M. Giovannozzi, “Multiturn Extraction: Performance Analysis of Old and New Approaches”, *CERN-PS (AE)* **2002-077** (2002).
- [8] P. J. Bryant, K. Johnsen, “Circular Accelerators and Storage Rings”, (Cambridge University Press, NY, 1993).
- [9] A. W. Chao, M. Tigner, “Handbook of Accelerator Physics and Engineering”, (World Scientific, Singapore, 1999) p. 253.
- [10] Courant and H. Snyder, *Ann. Phys.* **3**, (1958) 1.
- [11] J. Buon, “Beam Phase Space and Emittance” in *CERN* **94-01** p. 89 (1994).
- [12] A. W. Chao, M. Tigner, “Handbook of Accelerator Physics and Engineering”, (World Scientific, Singapore, 1999) p. 576.
- [13] R. Steerenberg, “Transverse emittance as a function of proton beam intensity”, *CERN PS (OP) Note* **2000-13** (2000).
- [14] A. Bazzani, E. Todesco, G. Turchetti, and G. Servizi, “A Normal Form Approach to the Theory of Nonlinear Betatronic Motion”, *CERN* **1994-02** (1994).
- [15] R. Cappi, M. Giovannozzi, M. Martini, “Some scenarios for preliminary tests of the new CT extraction”, *CERN PS (AE) Note* **2002-130** (2002).
- [16] O. Brüning, F. Willeke, in *4th European Particle Accelerator Conference*, edited by V. Suller and Ch. Petit-Jean-Genaz (World Scientific, Singapore, 1994) p. 991.
- [17] F. Zimmermann, in *4th European Particle Accelerator Conference*, edited by V. Suller and Ch. Petit-Jean-Genaz (World Scientific, Singapore, 1994) p. 327.
- [18] W. Fischer, M. Giovannozzi and F. Schmidt, *Phys. Rev. E* **55**, (3507) 1997.
- [19] A. J. Lichtenberg, M. A. Lieberman, “Regular and Chaotic Motion”, (Springer Verlag, Berlin, 1998).
- [20] R. Cappi, M. Giovannozzi, M. Martini, E. Métral, G. Métral, A.-S. Müller, R. Steerenberg, “Experimental Evidence of Adiabatic Trapping of Charged Particles in Stable Islands of Transverse Phase Space”, in preparation.
- [21] L. Sirovich, “Techniques of Asymptotic Analysis”, (Springer-Verlag, NY, 1971).

A Special functions

Most of the computations presented in this paper deal with the evaluation of 2D integrals involving Gaussian distributions. In this case it is customary to define the *error function* as the integral

$$\operatorname{erf}(z) = \frac{2}{\sqrt{\pi}} \int_0^z e^{-t^2} dt. \quad (12)$$

By using the normalisation property of the indefinite integral it is easy to prove that

$$\operatorname{erfc}(z) = 1 - \operatorname{erf}(z) = \frac{2}{\sqrt{\pi}} \int_z^{+\infty} e^{-t^2} dt. \quad (13)$$

The error function can be used also to express integrals involving the product of Gaussian distribution function and a polynomial. In particular, for the case of a second-order polynomial the following result is obtained using integration by parts

$$\int_0^z t^2 e^{-t^2} dt = -\frac{1}{2} z e^{-z^2} + \frac{\sqrt{\pi}}{4} \operatorname{erf}(z). \quad (14)$$

B Expression of first- and second-order moments for the slices of present CT

In the case of a plain Gaussian distribution (6) the analytical expression of the first- and second-order moments can be computed in closed form, also including the dependence on the relative position of the electrostatic septum.

- First slice: The computation of the first-order moments can be performed by directly applying the definition of central moments and by taking into account the shape of the domain of integration. By denoting with \hat{x}_0 the relative position of the electrostatic septum, the normalisation factor is given by

$$\mathcal{N} = \frac{1}{2\pi\epsilon} \int_{\hat{x}_0}^{+\infty} e^{-\frac{\hat{x}^2}{2\epsilon}} d\hat{x} \int_{-\infty}^{+\infty} e^{-\frac{\hat{x}'^2}{2\epsilon}} d\hat{x}' = \frac{1}{2} \operatorname{erfc}\left(\frac{\hat{x}_0}{\sqrt{2\epsilon}}\right). \quad (15)$$

Then, one obtains

$$\begin{aligned} \mu_{\hat{x}} &= \frac{1}{2\pi\epsilon} \frac{1}{\mathcal{N}} \int_{\hat{x}_0}^{+\infty} \hat{x} e^{-\frac{\hat{x}^2}{2\epsilon}} d\hat{x} \int_{-\infty}^{+\infty} e^{-\frac{\hat{x}'^2}{2\epsilon}} d\hat{x}' \\ &= \sqrt{\frac{2\epsilon}{\pi}} \frac{e^{-\frac{\hat{x}_0^2}{2\epsilon}}}{\operatorname{erfc}\left(\frac{\hat{x}_0}{\sqrt{2\epsilon}}\right)}, \end{aligned} \quad (16)$$

where the final results is obtained by applying the normalisation property and a change of variables to the original integral. Furthermore, $\mu_{\hat{x}'} = 0$ by symmetry.

The computation of the second-order moments gives:

$$\begin{aligned} \langle \hat{x}^2 \rangle &= \frac{1}{2\pi\epsilon} \frac{1}{\mathcal{N}} \int_{\hat{x}_0}^{+\infty} \hat{x}^2 e^{-\frac{\hat{x}^2}{2\epsilon}} d\hat{x} \int_{-\infty}^{+\infty} e^{-\frac{\hat{x}'^2}{2\epsilon}} d\hat{x}' - \mu_{\hat{x}}^2 \\ \langle \hat{x} \hat{x}' \rangle &= 0 \\ \langle \hat{x}'^2 \rangle &= \frac{1}{2\pi\epsilon} \frac{1}{\mathcal{N}} \int_{\hat{x}_0}^{+\infty} e^{-\frac{\hat{x}^2}{2\epsilon}} d\hat{x} \int_{-\infty}^{+\infty} \hat{x}'^2 e^{-\frac{\hat{x}'^2}{2\epsilon}} d\hat{x}' - \mu_{\hat{x}'}^2. \end{aligned} \quad (17)$$

With the help of some change of variables, together with the properties reported in Appendix A, the final result is obtained

$$\begin{aligned}
\langle \hat{x}^2 \rangle &= \epsilon \left[1 + \sqrt{\frac{2}{\pi}} \frac{\hat{x}_0}{\sqrt{\epsilon}} \frac{e^{-\frac{\hat{x}_0^2}{2\epsilon}}}{\operatorname{erfc}\left(\frac{\hat{x}_0}{\sqrt{2\epsilon}}\right)} - \frac{2}{\pi} \frac{e^{-\frac{\hat{x}_0^2}{\epsilon}}}{\operatorname{erfc}^2\left(\frac{\hat{x}_0}{\sqrt{2\epsilon}}\right)} \right] \\
\langle \hat{x} \hat{x}' \rangle &= 0 \\
\langle \hat{x}'^2 \rangle &= \epsilon.
\end{aligned} \tag{18}$$

– Second slice: In this case both $\mu_{\hat{x}}$ and $\mu_{\hat{x}'}$ are different from zero. The normalisation factor reads

$$\mathcal{N} = \frac{1}{2\pi\epsilon} \int_{-\infty}^{\hat{x}_0} e^{-\frac{\hat{x}^2}{2\epsilon}} d\hat{x} \int_{\hat{x}_0}^{+\infty} e^{-\frac{\hat{x}'^2}{2\epsilon}} d\hat{x}' = \frac{1}{4} \left[1 - \operatorname{erf}^2\left(\frac{\hat{x}_0}{\sqrt{2\epsilon}}\right) \right], \tag{19}$$

and the first-order moments are given by

$$\begin{aligned}
\mu_{\hat{x}} &= \frac{1}{2\pi\epsilon} \frac{1}{\mathcal{N}} \int_{-\infty}^{\hat{x}_0} \hat{x} e^{-\frac{\hat{x}^2}{2\epsilon}} d\hat{x} \int_{\hat{x}_0}^{+\infty} e^{-\frac{\hat{x}'^2}{2\epsilon}} d\hat{x}' \\
&= -\sqrt{\frac{2\epsilon}{\pi}} \frac{e^{-\frac{\hat{x}_0^2}{2\epsilon}}}{1 + \operatorname{erf}\left(\frac{\hat{x}_0}{\sqrt{2\epsilon}}\right)}
\end{aligned} \tag{20}$$

$$\begin{aligned}
\mu_{\hat{x}'} &= \frac{1}{2\pi\epsilon} \frac{1}{\mathcal{N}} \int_{-\infty}^{\hat{x}_0} e^{-\frac{\hat{x}^2}{2\epsilon}} d\hat{x} \int_{\hat{x}_0}^{+\infty} \hat{x}' e^{-\frac{\hat{x}'^2}{2\epsilon}} d\hat{x}' \\
&= \sqrt{\frac{2\epsilon}{\pi}} \frac{e^{-\frac{\hat{x}_0^2}{2\epsilon}}}{\operatorname{erfc}\left(\frac{\hat{x}_0}{\sqrt{2\epsilon}}\right)}.
\end{aligned}$$

The second-order moments, defined as

$$\begin{aligned}
\langle \hat{x}^2 \rangle &= \frac{1}{2\pi\epsilon} \frac{1}{\mathcal{N}} \int_{-\infty}^{\hat{x}_0} \hat{x}^2 e^{-\frac{\hat{x}^2}{2\epsilon}} d\hat{x} \int_{\hat{x}_0}^{+\infty} e^{-\frac{\hat{x}'^2}{2\epsilon}} d\hat{x}' - \mu_{\hat{x}}^2 \\
\langle \hat{x} \hat{x}' \rangle &= 0 \\
\langle \hat{x}'^2 \rangle &= \frac{1}{2\pi\epsilon} \frac{1}{\mathcal{N}} \int_{-\infty}^{\hat{x}_0} e^{-\frac{\hat{x}^2}{2\epsilon}} d\hat{x} \int_{\hat{x}_0}^{+\infty} \hat{x}'^2 e^{-\frac{\hat{x}'^2}{2\epsilon}} d\hat{x}' - \mu_{\hat{x}'}^2,
\end{aligned} \tag{21}$$

can be expressed in final form as

$$\begin{aligned}
\langle \hat{x}^2 \rangle &= \epsilon \left\{ 1 - \sqrt{\frac{2}{\pi}} \frac{\hat{x}_0}{\sqrt{\epsilon}} \frac{e^{-\frac{\hat{x}_0^2}{2\epsilon}}}{1 + \operatorname{erf}\left(\frac{\hat{x}_0}{\sqrt{2\epsilon}}\right)} + \frac{2}{\pi} \frac{e^{-\frac{\hat{x}_0^2}{\epsilon}}}{\left[1 + \operatorname{erf}\left(\frac{\hat{x}_0}{\sqrt{2\epsilon}}\right)\right]^2} \right\} \\
\langle \hat{x} \hat{x}' \rangle &= 0 \\
\langle \hat{x}'^2 \rangle &= \epsilon \left[1 + \sqrt{\frac{2}{\pi}} \frac{\hat{x}_0}{\sqrt{\epsilon}} \frac{e^{-\frac{\hat{x}_0^2}{2\epsilon}}}{\operatorname{erfc}\left(\frac{\hat{x}_0}{\sqrt{2\epsilon}}\right)} - \frac{2}{\pi} \frac{e^{-\frac{\hat{x}_0^2}{\epsilon}}}{\operatorname{erfc}^2\left(\frac{\hat{x}_0}{\sqrt{2\epsilon}}\right)} \right].
\end{aligned} \tag{22}$$

- Third slice: The results can be easily deduced from those for the second slice, by simply considering that both slices have the same shape, only the role of \hat{x} and \hat{x}' is exchanged, namely

$$\hat{x}_3 = -\hat{x}'_2 \quad \hat{x}'_3 = \hat{x}_2, \quad (23)$$

where the subscript stands for the slice number. The final result is:

$$\mu_{\hat{x},3} = -\mu_{\hat{x}',2} \quad (24)$$

$$\mu_{\hat{x}',3} = \mu_{\hat{x},2}$$

and

$$\begin{aligned} \langle \hat{x}^2 \rangle_3 &= \langle \hat{x}'^2 \rangle_2 \\ \langle \hat{x} \hat{x}' \rangle_3 &= -\langle \hat{x} \hat{x}' \rangle_2 \\ \langle \hat{x}'^2 \rangle_3 &= \langle \hat{x}^2 \rangle_2 \end{aligned} \quad (25)$$

- Fourth slice: In this case the normalisation factor equals

$$\mathcal{N} = \frac{1}{2\pi\epsilon} \int_{-\hat{x}_0}^{\hat{x}_0} e^{-\frac{\hat{x}^2}{2\epsilon}} d\hat{x} \int_{-\infty}^{-\hat{x}_0} e^{-\frac{\hat{x}'^2}{2\epsilon}} d\hat{x}' = \frac{1}{2} \operatorname{erf}\left(\frac{\hat{x}_0}{\sqrt{2\epsilon}}\right) \operatorname{erfc}\left(\frac{\hat{x}_0}{\sqrt{2\epsilon}}\right). \quad (26)$$

Furthermore, $\mu_{\hat{x}} \equiv 0$, while $\mu_{\hat{x}'}$ is given by

$$\mu_{\hat{x}'} = -\sqrt{\frac{2\epsilon}{\pi}} \frac{e^{-\frac{\hat{x}_0^2}{2\epsilon}}}{\operatorname{erfc}\left(\frac{\hat{x}_0}{\sqrt{2\epsilon}}\right)}. \quad (27)$$

Using these results, the values of the second-order moments are derived, namely

$$\begin{aligned} \langle \hat{x}^2 \rangle &= \frac{1}{2\pi\epsilon} \frac{1}{\mathcal{N}} \int_{-\hat{x}_0}^{\hat{x}_0} \hat{x}^2 e^{-\frac{\hat{x}^2}{2\epsilon}} d\hat{x} \int_{-\infty}^{-\hat{x}_0} e^{-\frac{\hat{x}'^2}{2\epsilon}} d\hat{x}' - \mu_{\hat{x}}^2 \\ \langle \hat{x} \hat{x}' \rangle &= 0 \\ \langle \hat{x}'^2 \rangle &= \frac{1}{2\pi\epsilon} \frac{1}{\mathcal{N}} \int_{-\hat{x}_0}^{\hat{x}_0} e^{-\frac{\hat{x}^2}{2\epsilon}} d\hat{x} \int_{-\infty}^{-\hat{x}_0} \hat{x}'^2 e^{-\frac{\hat{x}'^2}{2\epsilon}} d\hat{x}' - \mu_{\hat{x}'}^2. \end{aligned} \quad (28)$$

Hence

$$\begin{aligned} \langle \hat{x}^2 \rangle &= \epsilon \left[1 - \sqrt{\frac{2}{\pi}} \frac{\hat{x}_0}{\sqrt{\epsilon}} \frac{e^{-\frac{\hat{x}_0^2}{2\epsilon}}}{\operatorname{erf}\left(\frac{\hat{x}_0}{\sqrt{2\epsilon}}\right)} \right] \\ \langle \hat{x} \hat{x}' \rangle &= 0 \\ \langle \hat{x}'^2 \rangle &= \epsilon \left[1 + \sqrt{\frac{2}{\pi}} \frac{\hat{x}_0}{\sqrt{\epsilon}} \frac{e^{-\frac{\hat{x}_0^2}{2\epsilon}}}{\operatorname{erfc}\left(\frac{\hat{x}_0}{\sqrt{2\epsilon}}\right)} - \frac{2}{\pi} \frac{e^{-\frac{\hat{x}_0^2}{\epsilon}}}{\operatorname{erfc}^2\left(\frac{\hat{x}_0}{\sqrt{2\epsilon}}\right)} \right]. \end{aligned} \quad (29)$$

- Fifth slice: Due to the symmetries, $\mu_{\hat{x}}$ and $\mu_{\hat{x}'}$ are both equal to zero. Then, the computation of the second-order moments is quite simple. The final result reads:

$$\mathcal{N} = \frac{1}{2\pi\epsilon} \int_{-\hat{x}_0}^{\hat{x}_0} e^{-\frac{\hat{x}^2}{2\epsilon}} d\hat{x} \int_{-\hat{x}_0}^{\hat{x}_0} e^{-\frac{\hat{x}'^2}{2\epsilon}} d\hat{x}' = \operatorname{erf}^2\left(\frac{\hat{x}_0}{\sqrt{2\epsilon}}\right), \quad (30)$$

and

$$\begin{aligned}
\langle \hat{x}^2 \rangle &= \epsilon \left[1 - \sqrt{\frac{2}{\pi}} \frac{\hat{x}_0}{\sqrt{\epsilon}} \frac{e^{-\frac{\hat{x}_0^2}{2\epsilon}}}{\operatorname{erf}\left(\frac{\hat{x}_0}{\sqrt{2\epsilon}}\right)} \right] \\
\langle \hat{x} \hat{x}' \rangle &= 0 \\
\langle \hat{x}'^2 \rangle &= \langle \hat{x}^2 \rangle .
\end{aligned} \tag{31}$$

C Asymptotic behaviour of erfc

The analysis of the limiting behaviour of the Twiss parameters and emittance for the different slices of the old CT extraction, requires the knowledge of the asymptotic development of the function $\operatorname{erfc}(z)$ for $z \rightarrow +\infty$. By using the approach outlined in Ref. [21] it is possible to obtain such a development. The first step consists in recasting Eq. (13) in the form:

$$\operatorname{erfc}(z) = \frac{2}{\sqrt{\pi}} e^{-z^2} \int_0^{+\infty} e^{-2xz} e^{-x^2} dx. \tag{32}$$

Hence, the problem of finding the asymptotic development of $\operatorname{erfc}(z)$ is moved to the search of the asymptotic behaviour of the integral

$$\mathcal{I}(z) = \int_0^{+\infty} e^{-2xz} e^{-x^2} dx. \tag{33}$$

By using integration by parts it is possible to show that

$$\mathcal{I}(z) = \sum_{i=1}^N \frac{(-1)^{i-1}}{z^i} [\mathcal{F}_{i-1}(+\infty) \mathcal{G}_{-i}(+\infty) - \mathcal{F}_{i-1}(0) \mathcal{G}_{-i}(0)] + \mathcal{R}_N, \tag{34}$$

where \mathcal{R}_N is the remainder term and the functions \mathcal{F} , \mathcal{G} are defined through the recursions:

$$\mathcal{F}_0(x) = e^{-x^2} \quad \mathcal{F}_i(x) = \frac{d}{dx} \mathcal{F}_{i-1}(x) \tag{35}$$

$$\mathcal{G}_0(x) = e^{-2x} \quad \mathcal{G}_{-i}(x) = \int \mathcal{G}_{-i+1}(y) dy. \tag{36}$$

For the case under consideration, it is easy to prove by induction that

$$\mathcal{G}_{-i}(x) = \frac{(-1)^i}{2^i} e^{-2x} \tag{37}$$

$$\mathcal{F}_i(x) = (-1)^i H_i(x) e^{-x^2}, \tag{38}$$

where $H_i(x)$ is the Hermite polynomial of degree i in the variable x . By using the well-known properties

$$H_i(-x) = (-1)^i H_i(x) \tag{39}$$

$$H_{i+1}(x) = 2x H_i(x) - 2i H_{i-1}(x), \tag{40}$$

it is possible to prove that

$$\mathcal{F}_{2i+1}(0) = 0 \quad \forall i \quad (41)$$

$$\mathcal{F}_{2i}(0) = (-1)^i 2^i (2i - 1)!!$$

and the expression for the asymptotic development reads:

$$\operatorname{erfc}(z) \sim \frac{2}{\sqrt{\pi}} e^{-z^2} \sum_{i=0}^N \frac{(-1)^i (2i - 1)!!}{z^{2i+1} 2^{i+1}}. \quad (42)$$

D Asymptotic expansion of equivalent Twiss parameters for the slices of present CT

In the case of a plain Gaussian distribution (6), the presence of infinite tails make it possible to test the behaviour of equivalent Twiss parameters and extracted beam emittance when the relative position of the electrostatic septum is moved towards higher and higher amplitudes. By using the analytical expressions derived in Appendix B together with the asymptotic expansion of the erfc function reported in Appendix C, it is possible to obtain the asymptotic expansion for the mismatch parameter β_i/β and ϵ_i/ϵ . If ζ stands for $\hat{x}_0/\sqrt{\epsilon}$, then the following holds (the subscript of the various quantities stands for the slice number):

$$\langle \hat{x}_1^2 \rangle \sim \frac{\epsilon}{\zeta^2} \left(1 - \frac{5}{\zeta^2} \right) \quad \langle \hat{x}_2^2 \rangle \sim \epsilon \left(1 - \frac{\zeta e^{-\frac{\zeta^2}{2}}}{\sqrt{2\pi}} \right) \quad (43a)$$

$$\langle \hat{x}'_1{}^2 \rangle \sim \epsilon \quad \langle \hat{x}'_2{}^2 \rangle \sim \frac{\epsilon}{\zeta^2} \left(1 - \frac{5}{\zeta^2} \right) \quad (43b)$$

$$\frac{\bar{\beta}_1}{\beta} \sim \frac{1}{\zeta} \left(1 - \frac{2}{\zeta^2} \right) \quad \frac{\bar{\beta}_2}{\beta} \sim \zeta \left(1 + \frac{5}{2\zeta^2} \right) \quad (43c)$$

$$\epsilon_1 \sim \frac{\epsilon}{\zeta} \left(1 - \frac{3}{\zeta^2} \right) \quad \epsilon_2 \sim \frac{\epsilon}{\zeta} \left(1 - \frac{5}{2\zeta^2} \right), \quad (43d)$$

$$\langle \hat{x}_3^2 \rangle \sim \frac{\epsilon}{\zeta^2} \left(1 - \frac{5}{\zeta^2} \right) \quad \langle \hat{x}_4^2 \rangle \sim \epsilon \left(1 - \frac{2\zeta e^{-\frac{\zeta^2}{2}}}{\sqrt{2\pi}} \right) \quad (44a)$$

$$\langle \hat{x}'_3{}^2 \rangle \sim \epsilon \left(1 - \frac{\zeta e^{-\frac{\zeta^2}{2}}}{\sqrt{2\pi}} \right) \quad \langle \hat{x}'_4{}^2 \rangle \sim \frac{\epsilon}{\zeta^2} \left(1 - \frac{4}{\zeta^2} \right) \quad (44b)$$

$$\frac{\bar{\beta}_3}{\beta} \sim \frac{1}{\zeta} \left(1 - \frac{5}{2\zeta^2} \right) \quad \frac{\bar{\beta}_4}{\beta} \sim \zeta \left(1 + \frac{3}{2\zeta^2} \right) \quad (44c)$$

$$\epsilon_3 \sim \frac{\epsilon}{\zeta} \left(1 - \frac{5}{2\zeta^2} \right) \quad \epsilon_4 \sim \frac{\epsilon}{\zeta} \left(1 - \frac{3}{2\zeta^2} \right), \quad (44d)$$

$$\langle \hat{x}_5^2 \rangle = \epsilon_5 \sim \epsilon \left(1 - \sqrt{\frac{2}{\pi}} \zeta e^{-\frac{\zeta^2}{2}} \right). \quad (45)$$